Special Section: Soil–Plant–Atmosphere Continuum

Natalie Schröder*
Mathieu Javaux
Jan Vanderborght
Bernhard Steffen
Harry Vereecken

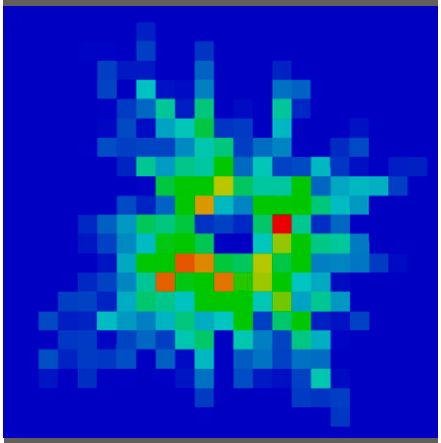

# Effect of Root Water and Solute Uptake on Apparent Soil Dispersivity: A Simulation Study

Plants take up water from the root zone and thus affect the three-dimensional water flow field and solute transport processes in the soil. In this study, the impacts of root architecture, plant solute uptake mechanisms (passive, active, and solute exclusion), and plant transpiration rate on the water flow field in the soil and on solute spreading were simulated. Therefore, a fully mechanistic model was used to simulate water flow along water potential gradients in the root–soil continuum by coupling a three-dimensional Richards equation in the soil with a flow equation in the root xylem vessels. Solute transport was simulated using a three-dimensional random walk particle tracking algorithm. To quantify the effect of root water and nutrient uptake on solute transport, an equivalent one-dimensional flow and transport model was fitted to horizontally averaged simulation results, and the fitted apparent parameters were compared with the parameters of the three-dimensional model. Our simulation results showed that the apparent dispersivity length is affected by the heterogeneous flow field, caused by root water uptake, and changed in a range of 50%, depending on solute redistribution in the root zone that depends on solute uptake type and soil dispersivity length. In addition, simulation results indicate that local concentration gradients within the root zone have an impact on apparent solute uptake rate parameters used in one-dimensional models to calculate uptake rates from spatially averaged concentrations. This shows the importance of small scale three-dimensional water and solute fluxes induced by root water and nutrient uptake.

Abbreviations: BTC, breakthrough curve; CDE, convection–dispersion equation; FE, finite element; PARTRACE, three-dimensional solute transport model in soil; RLD, root length density; R-SWMS, three-dimensional water flow model in soil and roots; RWPT, random walk particle tracking.

The migration of water and solutes within soils is significantly affected by the uptake of water and solutes by plants through their roots. This numerical study investigates the effect of variations in water and solute movement induced by individual roots on solute spreading, which is quantified by apparent dispersivity, in cropped soils.

Natalie Schröder and Bernhard Steffen, Jülich Supercomputing Centre, Institute of Advanced Simulation, Forschungszentrum Jülich GmbH, D-52425 Jülich, Germany; Mathieu Javaux, Jan Vanderborght, and Harry Vereecken, Institute of Bio- and Geoscience, Agrosphere Institute, IBG-3, Forschungszentrum Jülich GmbH, D-52425 Jülich, Germany. *Corresponding author (na.schroeder@fz-juelich.de).

Vadose Zone J.
doi:10.2136/vzj2012.0009
Received 18 Jan. 2012.



**Understanding the effect of root water uptake** on soil water flow and solute transport processes in the rhizosphere is fundamental for various agricultural problems, such as managing water and salt balances of irrigated fields and limiting leaching of pesticides (Green et al., 2006). The presence of plants affects solute fate not only because of the solute uptake itself (solute sink), but also because the plants affect the water velocity field by extracting water (water sink). Water uptake by plant roots decreases the water content in vegetated soil layers and disturbs the water velocity. For this reason, the vertical velocity and thus the transport velocity increase with depth, and the variability of the vertical and horizontal components of the velocity field changes, thus resulting in solute dispersion.

How plant water uptake influences solute spreading is still a subject of ongoing debate. An apparent increasing dispersivity due to plant roots in soil was described by Vogeler et al. (2001). In contrast, a decreasing dispersivity was reported by Gish and Jury (1983), who compared leaching experiments in cropped fields with a one-dimensional solute transport model. A similar effect was reported by Russo et al. (1998), who presented a numerical study for three-dimensional field-scale nutrient transport in heterogeneous, partially saturated soil and investigated transport of tracer and reactive solute. They detected a decreasing longitudinal nutrient spreading and a "skewing of the solute breakthrough." In their simulation study, they used a water sink term that is proportional to the soil conductivity times a root effectiveness function, which was assumed to be related to the root length density.

In soils with heterogeneous water distributions and when root hydraulic conductivities are low compared with the soil hydraulic conductivity, root water uptake is not proportional to the root length density (Javaux et al., 2008). Under such conditions, it is unclear how to determine the root water uptake distribution. This implies that numerical simulation studies that investigated the effect of root water uptake on transport processes in

heterogeneous soils in fact have relied on unverified assumptions. Another limitation of simulation studies that have been performed so far is that smooth root uptake functions were used. As a consequence, flow heterogeneity that is induced by flow to individual roots (i.e., when the root length density function becomes a binary function) could not be considered. Finally, when considering the effect of root activity on solute transport, plant uptake of solutes needs to be considered as well. Whether or not solutes are taken up by plants and to what extent will have an impact on the distribution of the solute mass in the heterogeneous flow field, which can have important consequences for transport processes in heterogeneous flow fields (Vanderborght et al., 1998; Vanderborght et al., 2006), and therefore on the transport process.

Studies based on numerical simulation have been used to assess the impact of various factors on solute fate, for example, soil heterogeneity (Hammel et al., 1999; Javaux et al., 2006; Russo et al., 2006) and solute chemical properties (Yang et al., 1996; Russo et al., 2004). Although a numerical study cannot replace real experimental data, it may be used to obtain insight on how different processes have an influence on transport. In numerical simulations, certain processes can be turned on or off, so that their impact can be highlighted. Numerical simulations are therefore useful to unravel sensitivities to certain processes, which may be difficult to obtain from real experiments. The advantage of one-dimensional models is their short calculation time. For large datasets and inverse simulation of measured data, they can be applied and run much faster than two- or three-dimensional models. But, neglected transport processes in the other spatial dimensions need to lumped in parameters of the one-dimensional models. However, today, other numerical models exist that explicitly account for the three-dimensional distribution of water and solute uptake at the centimeter scale, within the root zone of a single plant (including roots from adjacent plants). In contrast to one-dimensional models, three-dimensional models at plant scale (Javaux et al., 2008) have to deal with larger numbers of root and soil input parameters, but they rely on fewer assumptions about the spatial distribution of root and nutrient uptake (Draye et al., 2010).

In this study, we present numerical solute transport experiments and investigate how water and solute uptake by the plant affects the apparent dispersivity length, which is a parameter of a one-dimensional transport model that lumps the effect of the locally three-dimensional and variable transport process on solute spreading in the mean flow direction. Therefore, we used a model that explicitly couples water flow and nutrient uptake in a three-dimensional root structure with a three-dimensional model for water and solute transport in soil. In this model, water flow in the soil–root system is described in a fully mechanistic manner, thereby avoiding empirical relationships between root density, local soil water potential, and root water uptake that are typically used to represent root water uptake in soil water flow models. A validation of this approach to simulate water uptake was given by Doussan et al. (2006).

We start our simulations with very simplified setups. Single parameters like solute uptake type or the transpiration rate are modified. Afterward, parameters and initial and boundary conditions are adapted to describe more realistic conditions. The effect of water and nutrient uptake on the apparent dispersivity length are analyzed by fitting an effective one-dimensional transport model to horizontally averaged three-dimensional simulation results. Besides the influence of root water and nutrient uptake on the apparent dispersivity length, we also point out the importance of small-scale (approximately 1-cm resolution) flow and transport processes and small-scale variations in solute concentration in the effective parameterization of solute uptake in one-dimensional models.

# Theory

## Three-Dimensional Water Flow Model in Soil and Roots: R-SWMS

The three-dimensional water flow model in soil and roots, the R-SWMS model (Javaux et al., 2008; Schröder et al., 2008), couples a three-dimensional soil water flow model with a root water model. In the soil, the water flow is described by the Richards (1931) equation:

$$\frac{\partial \theta}{\partial t} = \nabla[\mathbf{K}(h)\nabla(h+z)] - S(x,y,z,t) \quad [1]$$

where $\theta$ ($cm^3\ cm^{-3}$) is the volumetric water content, $t$ (d) is time, $\mathbf{K}$ ($cm\ d^{-1}$) is the hydraulic conductivity tensor, $h$ (cm) is the matric head, $S$ ($d^{-1}$) is a sink term representing the root water uptake, and $z$ is the vertical coordinate (cm).

The soil flow equation is solved with a finite element (FE) Galerkin scheme (Simůnek et al., 1995).

The water flow in the root network is simulated by the model of Doussan et al. (2006), where the flow within the root xylem and between the soil–root interface and root xylem is solved by discretizing the root system as a network of connected root nodes. The radial soil–root water flow $J_r$ ($cm^3\ d^{-1}$) and the axial xylem flow $J_x$ ($cm^3\ d^{-1}$) in a root segment are defined by

$$J_r = K_r^* A_r \left(h_{s,int} - h_{xylem}\right) \qquad J_x = -K_x^* A_x \left(\frac{\Delta h_{xylem}}{l_{seg}} + \frac{\Delta z}{l_{seg}}\right) \quad [2]$$

with the radial root conductivity $K_r^*$ ($d^{-1}$), the root outer surface $A_r$ ($cm^2$), the xylem conductivity $K_x^*$ ($cm\ d^{-1}$), the xylem cross-sectional area $A_x$ ($cm^2$), the vertical coordinate $z$ (cm), the root segment length $l$ (cm), and the water pressure head at the soil–root interface $h_{int}$ (cm) and in the xylem $h_{xylem}$ (cm). At the soil–root interface, the water pressure head $h_{int}$ is computed by a

distance-based average of the water pressure head in the surrounding eight soil nodes:

$$h_{\text{int}} = \frac{\sum_{i=1}^{8} h_{i(1/\text{dist}_i)}}{\sum_{i=1}^{8} (1/\text{dist}_i)} \quad [3]$$

where dist is the distance from the root node to a soil node. Soil and root water flow are coupled via the sink term $S$ in the Richards equation (Eq. [1]). For a soil voxel $j$ the sink term is defined as

$$S_j = \frac{\sum_{k=1}^{n_k} J_{r,k}}{V_j} \quad [4]$$

where the radial fluxes of the root segments $k$, located in a soil voxel $k$, are summed up. Here, $V_j$ is the voxel volume, and $n_k$ is the number of root segments within voxel $j$.

Based on the initial soil water pressure head $h_{\text{int}}$, the root water model is solved. The resulting solution is used to calculate the water sink term for each soil voxel (Eq. [4]) for the Richards equation (Eq. [1]). The Richards equation and the root water flow model of Doussan are solved iteratively until a threshold error is reached.

## Three-Dimensional Solute Transport Model in Soil: PARTRACE

After calculating the water flow in soil and root, the three-dimensional convection–dispersion equation (CDE)

$$\frac{\partial \theta c}{\partial t} = \nabla(\theta \mathbf{D} \cdot \nabla c) - \nabla(\theta u c) - S' c \quad [5]$$

is solved, where $c$ (μmol cm$^{-3}$) is the solute concentration, $\mathbf{D}$ [cm$^2$ d$^{-1}$] is the dispersion coefficient tensor, $u$ (cm d$^{-1}$) is the pore water velocity (which is given by the solution of the Richards equation), and $S'$ [d$^{-1}$] is the solute sink term. The dispersion coefficient tensor for a three-dimensional isotropic porous medium (Bear, 1972) is given with

$$D_{ij} = \lambda_T \|u\| \delta_{ij} + (\lambda_L - \lambda_T) \frac{u_j u_i}{\|u\|} + D_w \tau \delta_{ij} \quad [6]$$

where $D_w$ (cm$^2$ d$^{-1}$) is the molecular diffusion coefficient in free water, $\tau$ is a tortuosity factor, $\delta_{ij}$ is the Kronecker delta function, $\lambda_L$ and $\lambda_T$ [cm] are the longitudinal and transverse dispersivities, respectively.

For the simulation of solute transport, the random walk particle tracking (RWPT) model PARTRACE (Bechtold et al., 2011) was used. In the RWPT algorithm, the CDE is defined as an equivalent stochastic differential equation (Tompson and Gelhar, 1990). This equation contains the velocity field obtained by the Richards equation and a random displacement for dispersion and is used to move a large number of solute particles, representing the solute mass, through the soil. Like every particle tracking method, PARTRACE is mass conservative by definition and is supposed to handle high concentration gradients, for example, at evaporation surfaces (Bechtold et al., 2011) and at root surfaces, when solutes are excluded by the plant or actively taken up, better then a FE method.

## Solute Sink Terms

For the root solute uptake term the definition of Hopmans and Bristow (2002) is adopted, where the nutrient uptake is summed up for every voxel of the soil grid and given in the sink term:

$$S' = \varepsilon S + (1 - \varepsilon) A \quad [7]$$

where $\varepsilon \in [0,1]$ is a partitioning coefficient. The first term on the right-hand side represents the passive solute uptake with water and contains the water sink term $S$ from the Richards equation (Eq. [1]). In the second term, the active solute uptake by the roots is defined by a Michaelis–Menten kinetic and a linear component

$$A = \left( \frac{V_{\max}}{K_m + c} + f \right) R_d \quad [8]$$

where $V_{\max}$ (μmol cm$^{-2}$ d$^{-1}$) is the maximum uptake rate per area of soil–root interface, $K_m$ (μmol cm$^{-3}$) the Michaelis–Menten constant, $R_d$ (cm$^2$ cm$^{-3}$) the root surface density, and $f$ the first-order rate coefficient (cm d$^{-1}$). $R_d$ is computed as follows:

$$R_d(x,y,z) = T_s \sigma'(x,y,z) \quad [9]$$

and is constant in time because root growth was not simulated. Here, $T_s$ (cm$^2$) is the total root surface at the current time, and the function $\sigma'$ describes the distribution of root surfaces within the spatial domain $\Omega$. The distribution $\sigma'$ is calculated in a voxel from the root surface of the root segments in the voxel around $(x,y,z)$ $\sigma(x,y,z)$ (cm$^2$) as:

$$\sigma' = \frac{\sigma(x,y,z)}{\int_\Omega \sigma(x,y,z) \, d\Omega} \quad [10]$$

By representing the root water uptake and solute uptake by sink terms in the soil water and solute transport models, the geometry, orientation, and location of a root segment in a soil voxel is not explicitly considered in the soil water and solute transport models. As a consequence, water pressure head and solute concentration variations toward root segments within the voxel are not resolved. Schröder et al. (2009) showed that this approach is valid for the water sink term and the pressure head distribution predictions as long as the voxel size is small enough (<1 cm). The effect of approximating the solute concentration at the soil root interface by the average concentration in the soil voxel will be evaluated using simulations with different voxel sizes.

# Materials and Methods

## Virtual Experiments

Virtual three-dimensional solute transport experiments under steady state flow conditions were generated with R-SWMS (for water velocity field) and PARTRACE (for solute transport) under different conditions.

### Soil Domain

For all scenarios a 24- by 24- by 60-cm soil column with lateral periodic boundary conditions was defined. With a discretization of 1 cm, the simulations where run with 38,125 soil nodes and 34,560 soil elements. The Mualem–van Genuchten expression (van Genuchten, 1980) were used to describe the $\theta(h)$ and $\mathbf{K}(h)$ relations. We used parameters representing hydraulic properties for loam (Table 1).

As top soil boundary condition for the water flow calculation, an infiltration rate of $J_w = -1$ cm d$^{-1}$ was chosen, and the bottom boundary was defined as free drainage. For the solute transport, a uniform solute step of $c_0 = 10^{-2}$ μmol cm$^{-3}$ was applied for the solute flux concentration (Table 2). The diffusion coefficient was defined as $D_w = 1$ cm$^2$ d$^{-1}$. The Michaelis–Menten parameters were selected from Roose and Kirk (2009) for nitrate uptake: $V_{max} = 0.044$ μmol cm$^{-2}$ d$^{-1}$, and $K_m = 0.05$ μmol cm$^{-3}$. Soil parameters for solute transport are shown in Table 3.The simulation time was 45 d and started at Day 45, which was the age of the simulated plants.

For our scenario definitions, three different types of solute uptake by the plant were specified: full passive solute uptake, full active solute uptake, and solute exclusion (no solute uptake) (Table 4).

By passive uptake, solute particles enter the plant only with water, by active uptake only by the Michaelis–Menten kinetic, and by solute exclusion, no solute is taken up.

## Plant Root Architecture

Two different plant root architectures were defined: fibrous and taprooted root systems (Fig. 1), with both plants being 45 d old. The root structures were created with Root Typ (Pagès et al., 2004) based on Italian ryegrass (*Lolium multiflorum* Lam.) and curled dock (*Rumex crispus* L.) architectural parameters. During the architecture generation, no spatial boundaries were defined for the root growth. If a root branch leaves the soil domain in the $x$ or $y$ direction, this root branch enters the soil domain again at the opposite site. This definition of a continuous root domain fits with the periodic boundary conditions of the soil domain. Thus, not only a lonely plant in a pot was simulated, but also the root branches from neighboring plants.

The fibrous and the taprooted system have an almost identically total root length of $3.1979 \times 10^3$ cm and $3.1976 \times 10^3$ cm, respectively.

Table 1. Parameters of hydraulic soil functions $\theta(h)$ and $K(h)$ for the Mualem– Genuchten expression (loam, Vanderborght et al., 2005): residual and saturated volumetric water content, $\theta_r$ and van $\theta_s$, respectively; van Genuchten–Mualem shape parameters, $\alpha$ and $n$; pore connectivity parameter $l$; saturated hydraulic conductivity $K_s$.

| $\theta_r$ | $\theta_s$ | $\alpha$ | $n$ | $l$ | $K_s$ |
|---|---|---|---|---|---|
| 0.08 | 0.43 | 0.04 cm | 1.6 | 0.5 | 50 cm d$^{-1}$ |

Table 2. Top and bottom soil boundary condition for water and solute simulations.

| Top boundary condition, water | Top boundary condition, solute | Bottom boundary condition |
|---|---|---|
| −1 cm d$^{-1}$ | $10^{-2}$ μmol cm$^{-3}$ | free drainage |

Table 3. Soil parameters for solute transport: longitudinal dispersivity length $\lambda_L$, transversal dispersivity length $\lambda_T$, molecular diffusion coefficient in free water $D_W$, tortuosity $\tau$.

| $\lambda_L$ | $\lambda_T$ | $D_W$ | $\tau$ |
|---|---|---|---|
| 1.0 cm | 0.1 $\lambda_L$ cm | 1.0 cm$^2$ d$^{-1}$ | $\theta^{3/7}/\theta_s^2$ |

Table 4. Solute uptake types: passive and active solute uptake and solute exclusion.

| Passive solute uptake | Active solute uptake | Solute exclusion |
|---|---|---|
| $S' = S$ | $S' = A$ | $S' = 0$ |

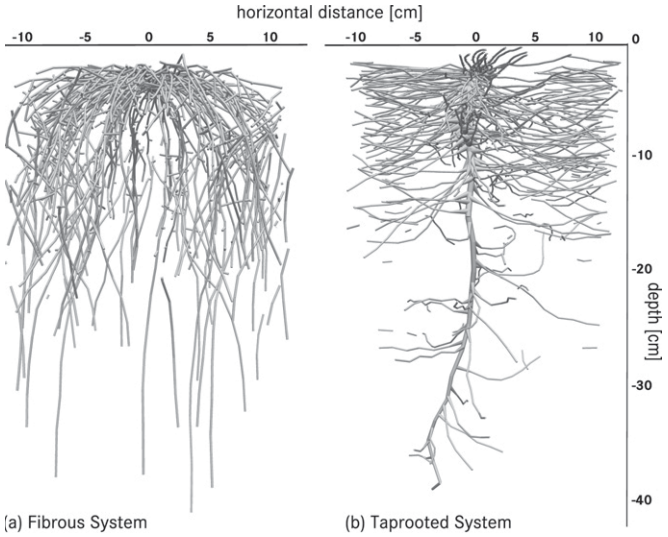


Fig. 1. Three-dimensional root architectures of (a) fibrous and (b) taprooted plants. Both were generated with Root Typ (Pagès et al., 2004); the root diameters shown are not to scale.

The total root surface is $1.211 \times 10^3$ cm$^2$ (fibrous) and $0.705 \times 10^3$ cm$^2$ (taprooted). Hence, the root length densities (RLD) of both structures are very similar (Fig. 2), but the root surface density is different, which is caused by the different root diameters of the roots

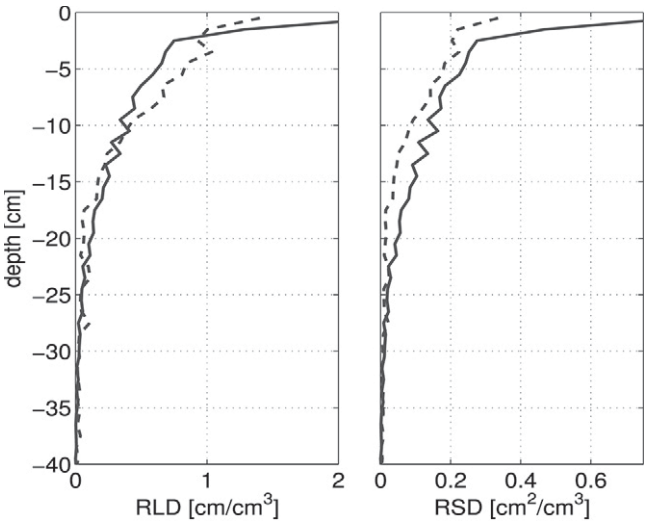


Fig. 2. Root length density (RLD) and root surface density (RSD) for the fibrous (continuous) and the taprooted (dashed) system.

of the two different plants. The root diameters are also given by Root Typ and vary between 0.014 and 1.082 cm for the taprooted and between 0.049 and 0.15 cm for the fibrous plant. The rhizosphere was not explicitly modeled because soil voxels around the roots were not described with different soil parameters.

For both plants, hydraulic characteristics were assumed to be constant in time and partly adapted from Doussan et al. (2006) (Table 5). Root properties were adapted following the branching order. A high axial root conductance of $K_x = K_x^* A_x = 4.32$ cm$^3$ d$^{-1}$ was set for all branching orders, so the water uptake could be expected to be similar to the root length density. Radial root conductivity was set to $L_r^* = 0.0648 \times 10^{-3}$ d$^{-1}$ for first branching order, $L_r^* = 0.181 \times 10^{-3}$ d$^{-1}$ for second and third branching order.

## Scenario Definitions

To investigate the effects of plants on solute transport in soil, four scenarios with different levels of complexity in the boundary conditions were used. They allow analysis of the impact of the solute uptake type, the transpiration rate, the soil dispersivity length $\lambda_L$, the transient flow conditions, and the plant root architecture on the apparent dispersivity length $\lambda_{app}$.

### Scenario 1: Impact of Solute Uptake Types

A constant transpiration rate with $T_{pot}$ (0.5 cm d$^{-1}$), equal to one-half of the constant irrigation rate, was chosen. Infiltration and transpiration were simulated for a specified time period until a water flow steady-state condition was reached. Then, a uniform solute step was applied to the upper soil surface. This scenario was run for all three solute uptake types (Table 4).

Table 5. Plant hydraulic parameters, partly adapted from Doussan et al. (2006): radial root conductivity $K_r^*$, xylem conductance.

| | First order | Second order | Third order |
|---|---|---|---|
| $K_r^*$, d$^{-1}$ | $0.0648 \times 10^{-3}$ | $0.181 \times 10^{-3}$ | $0.181 \times 10^{-3}$ |
| $K_x$, cm$^3$ d$^{-1}$ | 4.32 | 4.32 | 4.32 |

### Scenario 2: Impact of Transpiration Rate

In this scenario, various transpiration rates $T1_{pot} = 0.25$ cm d$^{-1}$, $T2_{pot} = 0.5$ cm d$^{-1}$, and $T3_{pot} = 0.667$ cm d$^{-1}$ were considered for passive uptake and solute exclusion.

### Scenario 3: Impact of Soil Dispersivity Length

In this third scenario, the impact of soil dispersivity length was investigated by changing $\lambda_{app}$ to 0.5, 1.0, and 2.0 cm. Water flow conditions where defined equal to Scenario 1, and a passive nutrient sink term and solute exclusion were considered.

### Scenario 4: Impact of Transient Flow

The impact of transient water flow was tested for solute exclusion (no solute uptake by roots). Time-averaged transpiration rate $T_{pot}$ was defined as one-half the constant irrigation, as in Scenario 1, but with a diurnal cycle for root water uptake. For the diurnal cycle, a jump function was chosen (Fig. 3). This jump function has maxima at $t = 0.5, 1.5, \ldots$ d (corresponding to midday) and zero between $t = x.25$ d and $x.75$ d (at night). During the day the horizontally averaged water flux may be upward close to the soil surface around noon, but the time average flux over the entire day remains negative and downward. By comparing the results with those of Scenario 1, the impact of transient flow could be analyzed.

## Scenario Analysis

The workflow of the scenario simulations and scenario analysis are schematized in Fig. 4. To derive $\lambda_{app}$, which characterizes solute spreading in an effective one-dimensional transport model, breakthrough curves (BTC) of horizontally averaged resident concentrations were calculated at different depths ($z = -10, -20, -40$ cm). The averaged concentrations at a certain depth were calculated as:

$$c = \frac{\sum_{i=1}^{N} c_i \theta_i \mathrm{vol}_i}{\sum_{i=1}^{N} \theta_i \mathrm{vol}_i} \qquad [11]$$

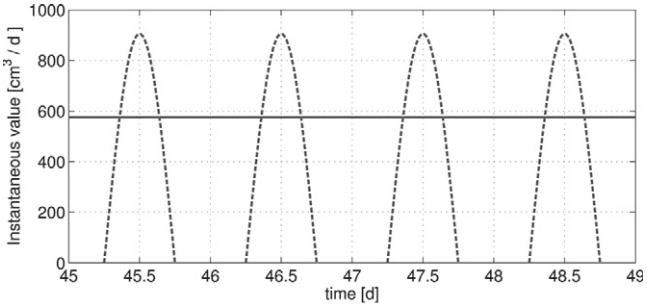


Fig. 3. Jump function for day-night transpiration flow (dashed) and irrigation flow (continuous line).

where $N$ is the number of soil grid voxels at a given plane and $c_i$, $\theta_i$, and $vol_i$ are the voxel resident concentration, the voxel water content, and the voxel volume, respectively. Depth profiles of horizontally averaged water sink term, water content, water flux, and pressure head were calculated from the R-SWMS output. The depth profile of the averaged three-dimensional sink term was used as one-dimensional sink term profile, and the averaged one-dimensional pressure head was defined as initial pressure head in the HYDRUS-1D simulations (Simůnek et al., 2008). These initial pressure heads remained unchanged for steady boundary conditions, which shows that the average water profiles from three-dimensional and the water profiles from one-dimensional were equal. The diffusion coefficient was imposed similarly to the three-dimensional simulations ($D_w$ = 1 cm$^2$ d$^{-1}$). For active solute uptake, the same Michaelis–Menten constant ($K_m$ = 0.05 μmol cm$^{-3}$) was used in HYDRUS-1D, the maximal uptake rate $V_{max}$ had to be adapted (see "Results: Solute Transport" below). Only the apparent dispersivity length was derived from fitting HYDRUS-1D to the breakthrough curves of horizontally averaged PARTRACE simulated solute concentrations. In addition, the same grid size (1 cm) was used for the effective one-dimensional transport model. The effect of the grid size on $\lambda_{app}$ and solute uptake was tested by changing the grid resolution to a finer (0.5 cm) and a coarser (1.5 cm) grid (not shown). The fitted dispersivity length $\lambda_{app}$ were in the same range for the finer grid (maximal difference: 0.088 cm). Therefore, simulations with 1-cm resolution were used in the comparison.

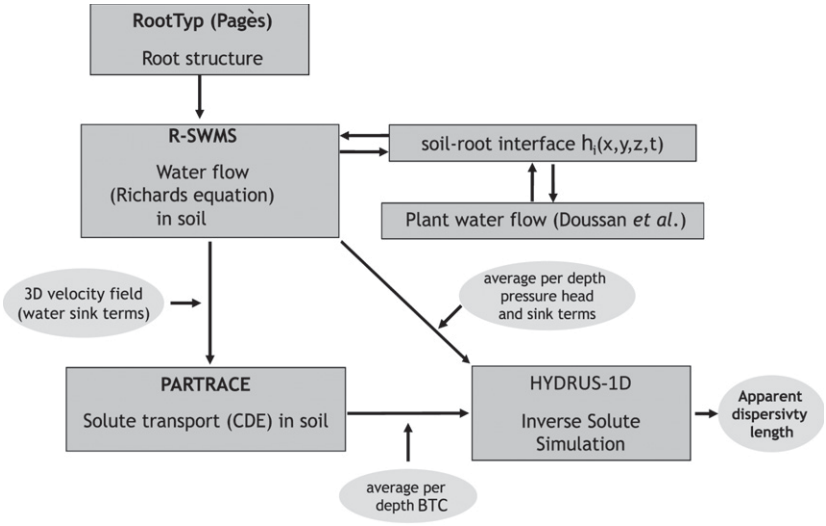


Fig. 4. Workflow of virtual solute transport experiments and their scenario analysis.

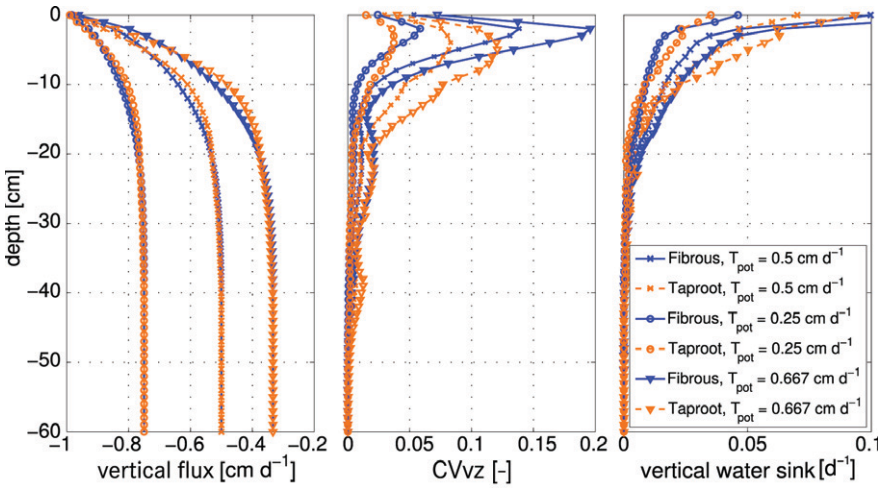


Fig. 5. Average flux profile, coefficient of variation of the vertical velocity component (CVvz), and average water sink profiles for three different transpiration rates: T1pot = 0.25 cm d$^{-1}$, T2pot = 0.5 cm d$^{-1}$, and T3pot = 0.6667 cm d$^{-1}$ for the fibrous (blue) and the taprooted (red) plant; water flux at the top: $J_w$ = −1 cm d$^{-1}$.

## Results: Steady-State Water Flow

Vertical profiles of the flux (averaged per depth), the coefficient of variation of the vertical velocity component and the vertical water sink term are compared for the different transpiration scenarios and both root architectures in Fig. 5. For a given root architecture, the flux, water sink and coefficient of variation of the pore water velocity profiles have similar shapes for the different transpiration rates. Only small differences in flux, sink term, and coefficient of variation of the pore water velocity between the fibrous and the taprooted plant were seen at the upper 30 cm of the soil column. Below the 30-cm soil depth, the profiles of both plants were similar due to the absence of roots in these soil layers. With higher transpiration rate, coefficient of variation of the pore water velocity and sink term increased, while the vertical velocity decreased. Since the dispersivity length is affected by the velocity spatial distribution and correlated to squared coefficient of variation of the vertical velocity, the highest apparent dispersivity length could be expected for the highest transpiration rate.

The three-dimensional distributions of the water content (Fig. 6a, 6b, 6c, 6d), the water sink term (Fig. 6f, 6 g, 6h, 6i), and the horizontal and vertical flux (Fig. 7) differed significantly between both root architectures. Note ,however, that the variability of the simulated water content was small (around 1%) when compared with the variability in water content observed in field soils (up to 10%, Vereecken et al., 2007). This might lead to different solute breakthrough curves for both plants, even if the average one-dimensional water content, the average water sink term and the vertical flux profiles were very similar for the taprooted

and for the fibrous root structure. In addition, the lateral fluxes to the roots (Fig. 7) cannot be represented with a one-dimensional model. Thus, the one-dimensional and the three-dimensional water flow and solute transport simulations may result in different predictions solute transport.

## Results: Solute Transport

### Scenario 1: Impact of Solute Uptake Type

The simulated BTCs for the solute uptake scenarios are given in Fig. 8. Each subfigure corresponds to one of the three different types of solute sink terms. The BTC is plotted at three depths ($z$ = −10, −20, or −40 cm) for the fibrous plant (blue) and the taproot plant (red). First it is observed that equilibrium concentration level changes with solute uptake type and depth. In case of nutrient exclusion (Fig. 8a), when one-half of the water is taken up by the plant, an increase of solute concentration in the pore water is obtained, which is twice the initial concentration below the root zone. The level of the equilibrium concentration reached in the effluent will therefore reflect the depth-integrated proportion of water that is extracted by the plant. In the case of passive uptake (Fig. 8b), the laterally averaged relative solute concentration should always be one since solute is taken up proportionally to the extracted water rate. In the case of active uptake (Fig. 8c), when solute is extracted at a larger rate than the corresponding passive nutrient uptake with the water, relative soil solute concentration should be lower than one. In addition, the solute concentration level decreased with depth for both plants. These results are consistent with the result obtained by Šimůnek and Hopmans (2009), where the root zone solute concentration decreased with active solute uptake, increased with solute exclusion, and did not change when nutrient uptake was passive.

The large difference between the two root architectures was only slightly reflected in the slope of the BTCs with passive nutrient uptake and solute exclusion, but the equilibrated solute amount differed between the two different root types for the exclusion scenario. In particular in the upper layer, the fibrous system approached a lower averaged concentration level than the taprooted system when solute was excluded. Since the equilibrium concentration in the effluent is related to root water uptake from the soil layer between the surface and the depth where solute breakthrough is observed, this shows that in the upper soil (from 0 to −10 cm), the two types of plants extracted different amounts of water. Figure 9 shows the spatial distribution of the solute

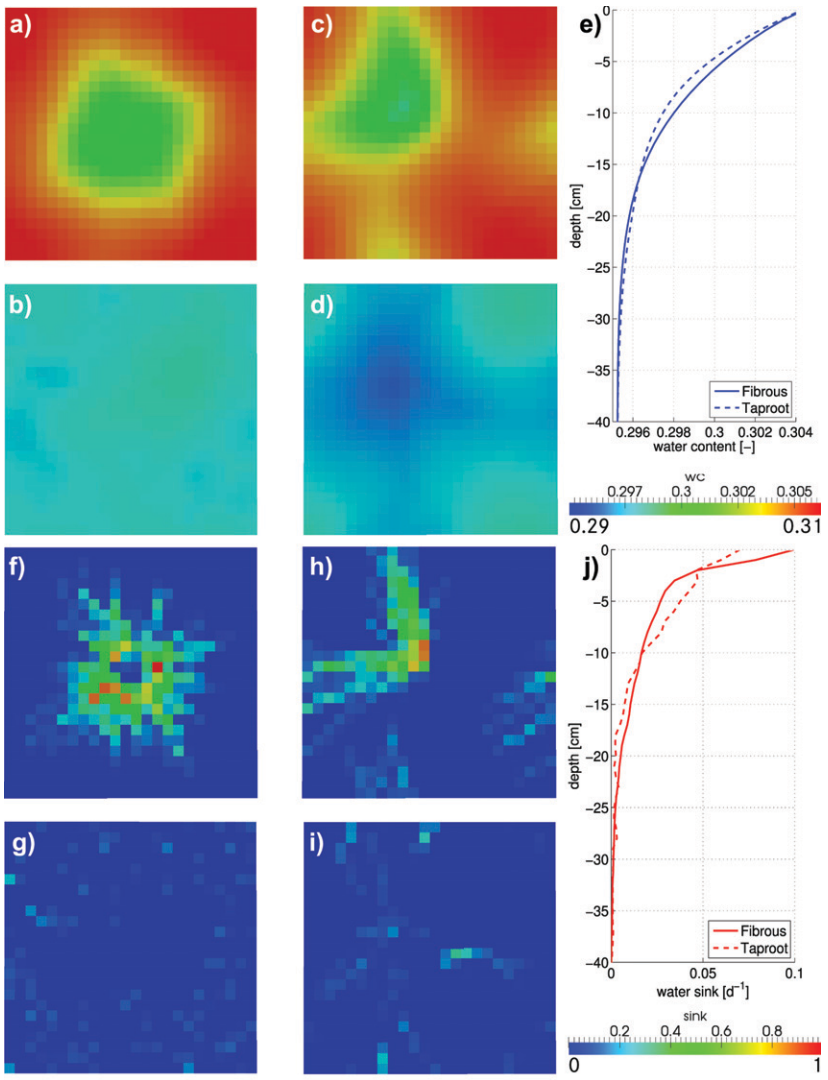


Fig. 6. Two-dimensional $x$–$y$ planes of the (a, b, c, d) water content and (f, h, g, i) water sink term distribution for the (a, b, f, g) fibrous plant at (a,b, f,g) $z$ = 0 cm and $z$ = −10 cm and (c, d, h, i) taprooted plant at (c,d, h,i) $z$ = 0 cm and $z$ = −10 cm; averaged (per depth) (e) water content profile and (j) water sink term profile.

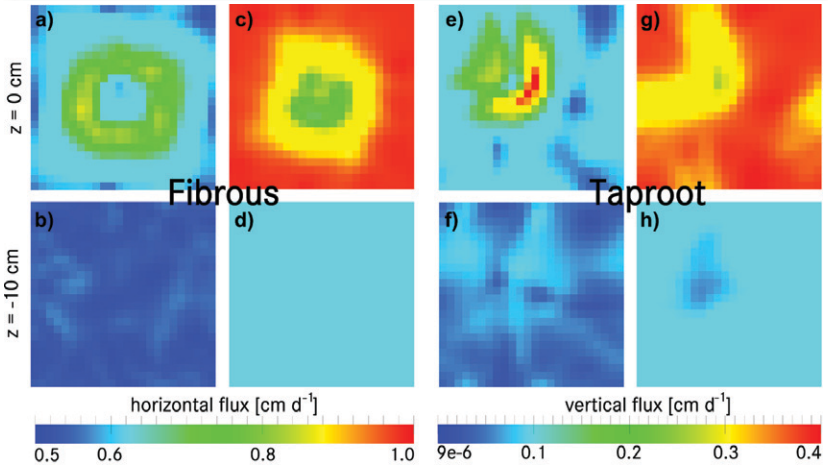


Fig. 7. Two-dimensional $x$–$y$ planes of the (a, b, e, f) horizontal and (c, d, g, h) vertical flux distributions for the (a, b, e, f) fibrous plant at (a,b, e,f) $z$ = 0 cm and $z$ = −10 cm and (c, d, g, h) taprooted plant at (c,d, g,h) $z$ = 0 cm and $z$ = −10 cm.

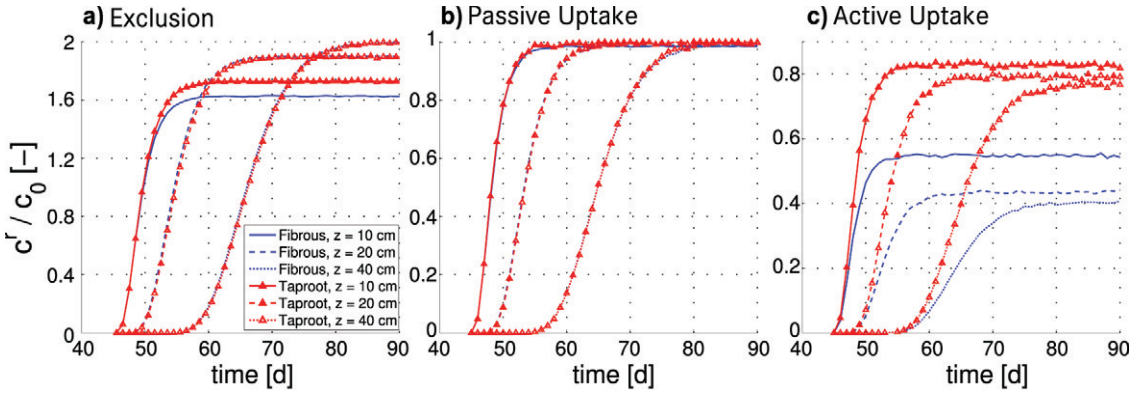


Fig. 8. Three-dimensionally simulated breakthrough curves at $z = -10, -20$, and $-40$ cm of the soil column with root water uptake by a fibrous and a taprooted plant structure; water flux at the top: $J_w = -1$ cm d$^{-1}$, transpiration rate $T_{pot} = 0.5$ cm d$^{-1}$; solute boundary condition at the top: $c_0 = 10^{-2}$ μmol cm$^{-3}$. The scenario was run with three different solute uptake types: solute exclusion and passive and active solute uptake.

concentration in the root zone at −15 cm depth, indicating an increase of solute concentration close to the root surface. While the local concentration increased mainly around the biggest root of the taprooted plant, solute accumulated more uniformly when the fibrous plant was considered, due to more uniform root distribution and water uptake.

In contrast to the passive solute uptake, more solute was removed from the soil column with active solute uptake. In this scenario a big difference can be seen between the fibrous and the taprooted plant. The breakthrough curves with the fibrous root system reached a lower equilibrium concentration level than the taprooted system. This is due to a high total root surface of the fibrous plant, leading to a higher nutrient uptake.

The apparent dispersivity lengths obtained by HYDRUS-1D are shown in Fig. 10 for three different solute uptake types. The standard error for all fitted, apparent dispersivity length $\lambda_{app}$ are shown in Tables 6 through 11.

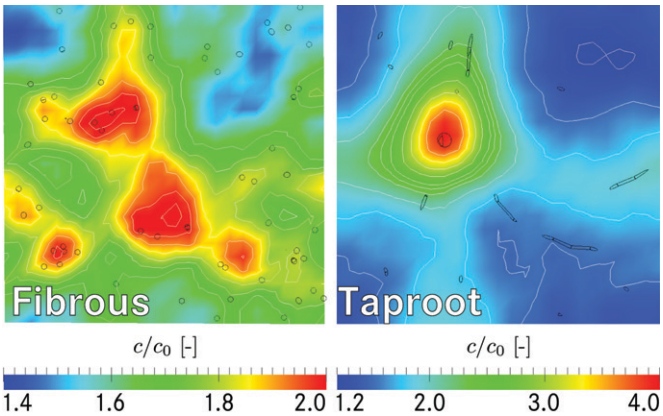


Fig. 9. Two-dimensional $x$–$y$ planes of the local concentration (solute exclusion), scaled to the initial concentration, at $z = -15$ cm for the (left) fibrous and (right) taprooted plant; the circles represent the plant roots.

Fitting the BTCs with the active solute uptake using the same values of the Michaelis–Menten parameter from the three-dimensional simulation in the one-dimensional model was not possible. When using the same values of the Michaelis–Menten parameter in one-dimensional and three-dimensional models, different concentration plateaus were simulated for active solute uptake (Fig. 11). This effect occurs because the three-dimensional model takes the local concentration at the soil root surface for the nutrient uptake into account. Since the active uptake in this scenario was larger

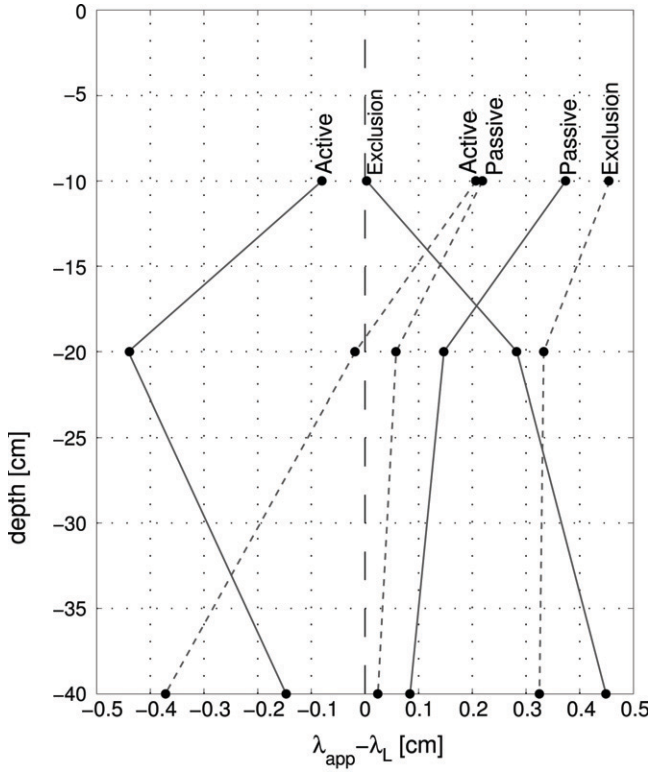


Fig. 10. Difference of apparent dispersivity length $\lambda_{app}$ minus soil dispersivity length $\lambda_L$ for different solute uptake types at three soil depths ($z = -10, -20, -40$ cm); fibrous system (continuous) and taprooted system (dashed).

Table 6. Apparent dispersivity length $\lambda_{app}$ fitted with HYDRUS-1D under steady-state conditions for solute exclusion, active and passive solute uptake, with transpiration rate in centimeters per day and the fibrous root system.

| | Exclusion | Passive | Active |
|---|---|---|---|
| $z = -10$ cm | $1.033 \pm 0.002$, $R^2 = 0.99681$ | $1.374 \pm 0.002$, $R^2 = 0.99736$ | $0.920 \pm 0.002$, $R^2 = 0.99005$ |
| $z = -20$ cm | $1.283 \pm 0.001$, $R^2 = 0.99902$ | $1.147 \pm 0.048$, $R^2 = 0.99836$ | $0.559 \pm 0.014$, $R^2 = 0.99278$ |
| $z = -40$ cm | $1.449 \pm 0.001$, $R^2 = 0.99885$ | $1.084 \pm 0.000$, $R^2 = 0.99934$ | $0.853 \pm 0.001$, $R^2 = 0.99700$ |

Table 7. Apparent dispersivity length $\lambda_{app}$ fitted with HYDRUS-1D under steady-state conditions for solute exclusion, active and passive solute uptake, with transpiration rate in centimeters per day and the taprooted root system.

| | Exclusion | Passive | Active |
|---|---|---|---|
| $z = -10$ cm | $1.456 \pm 0.001$, $R^2 = 0.99817$ | $1.219 \pm 0.001$, $R^2 = 0.99730$ | $1.207 \pm 0.002$, $R^2 = 0.99552$ |
| $z = -20$ cm | $1.333 \pm 0.001$, $R^2 = 0.99892$ | $1.058 \pm 0.000$, $R^2 = 0.99863$ | $0.982 \pm 0.001$, $R^2 = 0.99742$ |
| $z = -40$ cm | $1.325 \pm 0.001$, $R^2 = 0.99924$ | $1.024 \pm 0.000$, $R^2 = 0.99934$ | $0.628 \pm 0.001$, $R^2 = 0.99892$ |

Table 8. Apparent dispersivity length $\lambda_{app}$ for the fibrous plant, fitted with HYDRUS-1D under steady-state conditions, with solute exclusion with three transpiration rates, and the fibrous root system..

| | $T_{pot} = 0.25$ cm d$^{-1}$ | $T_{pot} = 0.5$ cm d$^{-1}$ | $T_{pot} = 0.667$ cm d$^{-1}$ |
|---|---|---|---|
| $z = -10$ cm | $1.090 \pm 0.001$, $R^2 = 0.99865$ | $1.033 \pm 0.002$, $R^2 = 0.99681$ | $1.195 \pm 0.002$, $R^2 = 0.99673$ |
| $-20$ cm | $1.191 \pm 0.001$, $R^2 = 0.99937$ | $1.283 \pm 0.001$, $R^2 = 0.99902$ | $1.417 \pm 0.002$, $R^2 = 0.99836$ |
| $-40$ cm | $1.188 \pm 0.000$, $R^2 = 0.99963$ | $1.449 \pm 0.001$, $R^2 = 0.99885$ | $1.672 \pm 0.001$, $R^2 = 0.99746$ |

Table 9. Apparent dispersivity length $\lambda_{app}$ for the fibrous plant, fitted with HYDRUS-1D under steady-state conditions, with passive solute uptake, with three transpiration rates, and the fibrous root system.

| | $T_{pot} = 0.25$ cm d$^{-1}$ | $T_{pot} = 0.5$ cm d$^{-1}$ | $T_{pot} = 0.667$ cm d$^{-1}$ |
|---|---|---|---|
| $z = -10$ cm | $1.190 \pm 0.001$, $R^2 = 0.99848$ | $1.456 \pm 0.001$, $R^2 = 0.99736$ | $1.830 \pm 0.004$, $R^2 = 0.99560$ |
| $z = -20$ cm | $1.180 \pm 0.001$, $R^2 = 0.99920$ | $1.333 \pm 0.001$, $R^2 = 0.99836$ | $1.525 \pm 0.001$, $R^2 = 0.99675$ |
| $z = -40$ cm | $1.160 \pm 0.000$, $R^2 = 0.99962$ | $1.325 \pm 0.001$, $R^2 = 0.99934$ | $1.507 \pm 0.001$, $R^2 = 0.99866$ |

Table 10. Apparent dispersivity length $\lambda_{app}$ fitted with HYDRUS-1D with steady-state and transient transpiration rate, solute exclusion, and the fibrous root system.

| $T_{pot} = 0.5$ cm d$^{-1}$ | Constant | Diurnal |
|---|---|---|
| $z = -10$ cm | $1.033 \pm 0.002$, $R^2 = 0.99736$ | $1.467 \pm 0.001$, $R^2 = 0.99665$ |
| $z = -20$ cm | $1.283 \pm 0.001$, $R^2 = 0.99836$ | $1.474 \pm 0.001$, $R^2 = 0.97555$ |
| $z = -40$ cm | $1.449 \pm 0.001$, $R^2 = 0.99934$ | $1.368 \pm 0.001$, $R^2 = 0.94804$ |

Table 11. Apparent dispersivity length $\lambda_{app}$ fitted with HYDRUS-1D, with steady-state and transient transpiration rate, solute exclusion, and the taprooted root system.

| $T_{pot} = 0.5$ cm d$^{-1}$ | Constant | Diurnal |
|---|---|---|
| $z = -10$ cm | $1.546 \pm 0.001$, $R^2 = 0.99817$ | $1.223 \pm 0.001$, $R^2 = 0.98262$ |
| $z = -20$ cm | $1.333 \pm 0.001$, $R^2 = 0.99892$ | $1.372 \pm 0.001$, $R^2 = 0.98973$ |
| $z = -40$ cm | $1.325 \pm 0.001$, $R^2 = 0.99924$ | $1.342 \pm 0.001$, $R^2 = 0.98906$ |

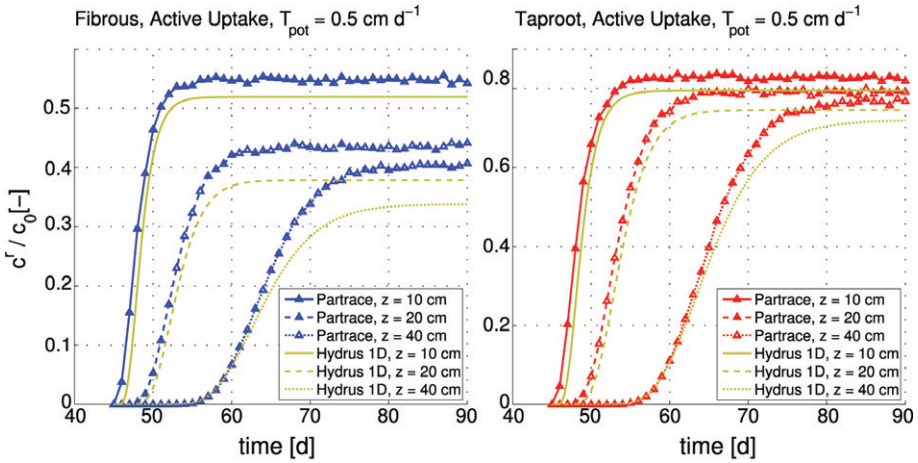


Fig. 11. Three-dimensionally simulated breakthrough curve of PARTRACE (blue, fibrous plant; red, taprooted plant) and HYDRUS-1D without fitting (green) at $z = -10$, $-20$, and $-40$ cm of the soil column with root water and active solute uptake; the scenario was run with $T_{pot} = 0.5$ cm d$^{-1}$.

than the uptake that would be expected for passive uptake (solute concentration levels were smaller than the applied concentration $c_0$), solute concentrations at a certain depth at the soil root interface were smaller than the average concentration at that depth. Since uptake in the one-dimensional model is calculated on the basis of average concentrations, the calculated uptake rate in the one-dimensional model is larger than in the three-dimensional model. These local concentrations vary, for example, due to solute uptake by the plant roots, and cannot be represented in one dimension. Therefore, the solute uptake rate $V_{max}$ in the one-dimensional model must also be adapted so as to match the simulated BTCs. The obtained values were $V_{max}$ = 0.066 cm$^2$ d$^{-1}$ for the fibrous plant and $V_{max}$ = 0.04 cm$^2$ d$^{-1}$ for the taprooted plant.

The effect of plant water uptake on the apparent dispersivity length was the largest for the solute exclusion scenario. An increase of the apparent dispersivity values with increasing depth was observed in the root zone of the taprooted plant, whereas a decrease was observed for the fibrous root system. For the taprooted system, the largest apparent dispersivity lengths were observed at the bottom of the root zone, despite the fact that the coefficient of variation of the vertical pore water velocity decreased to small values at this depth (Fig. 5).

In contrast, the highest $\lambda_{app}$ were observed at the top of the root zone for the passive uptake case, and the effect of passive solute uptake decreased below the root zone. This corresponds to the largest coefficient of variation of the vertical pore water velocity at the upper soil domain, which also decreased with depth (Fig. 5).

For the scenarios with active uptake, the apparent dispersivity length was smaller than the soil dispersivity length used in the three-dimensional simulations (Fig. 10). For these scenarios, the solute concentrations were the smallest around the roots, where also the largest deviations in the vertical pore water velocities were simulated. As a consequence, most of the solute mass that passed the root zone for this scenario was transported in a region where the variability in pore water velocity induced by the roots was small.

## Scenario 2: Impact of Transpiration Rate

In Scenario 2, both plants had similar impact on solute movement, so the results are shown for the fibrous root system only. In Fig. 12, the breakthrough curves for the three transpiration rates—one-quarter (T1), one-half (T2), and two-third (T3) of the total irrigation—with no nutrient uptake (blue) and passive solute uptake (red) are plotted versus the pore volume (cumulative outflow divided by the water volume in the soil between the soil surface and the depth where the BTC is simulated).

The difference between the passive solute uptake and the solute exclusion scenario is manifested by the different impact of the transpiration rate on $\lambda_{app}$. Despite the fact that the coefficient of variation of the vertical pore water velocity increased with

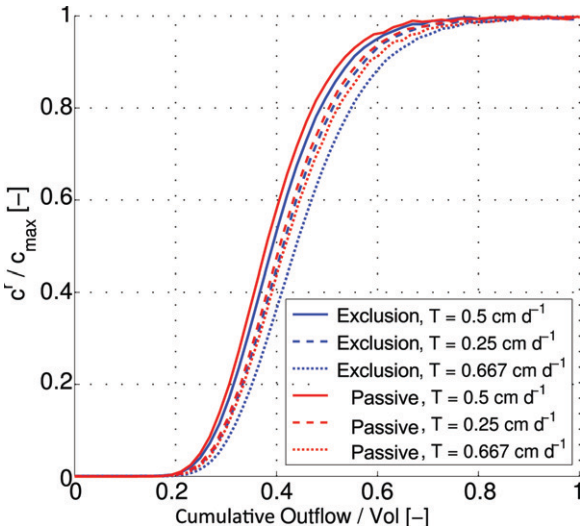


Fig. 12. Three-dimensionally simulated breakthrough curves for three different transpiration rates ($T_{pot}$ = 0.5, 0.25, 0.667 cm d$^{-1}$) at depth $z$ = −40 cm of the soil column with root water uptake by a fibrous plant; solute exclusion (blue) and passive solute uptake (red); the concentration is scaled to its maximum and compared to the cumulative water outflow.

increasing transpiration rate, the apparent dispersivity length decreased with increasing transpiration rate for the passive solute uptake scenario (Fig. 13). This shows that for passive solute uptake the dispersivity length is correlated to the variation of the velocity field, considering soil depth. However, values lower than the soil dispersivity length $\lambda$ = 1 cm are obtained. From this it follows that the coefficient of variation of the pore water velocity is not the main influence of the dispersivity length anymore when nutrients are taken up passively. Besides the coefficient of variation of the pore water velocity, the dispersivity length is also determined by the spatial correlation of the velocity field. A higher transpiration rate and root water uptake leads to larger horizontal water fluxes, which reduces the spatial correlation in the mean flow direction of the vertical water velocity and therefore the apparent dispersivity length. A similar effect of transient flow conditions and root water uptake on lateral solute redistribution and apparent dispersivity was observed in simulations by Russo et al. (1998).

On the other hand, for the scenario with solute exclusion, the apparent dispersivity length increased with transpiration rate. This indicates that the solute redistribution and accumulation of solute close to the soil root interface in this scenario had an important but different impact on the transport process than did the variability of pore water velocity induced by root water uptake.

## Scenario 3: Impact of Soil Dispersivity Length

To investigate the impact of the soil dispersivity length $\lambda_{app}$ used in the three-dimensional simulations we ran Scenario 1 with the fibrous root system, a transpiration rate of $T_{pot}$ = 0.5 cm d$^{-1}$, solute exclusion and passive solute uptake, and for several soil dispersivity lengths ($\lambda_{app}$ = 0.5, 1.0, and 2.0 cm). Figure 14 shows

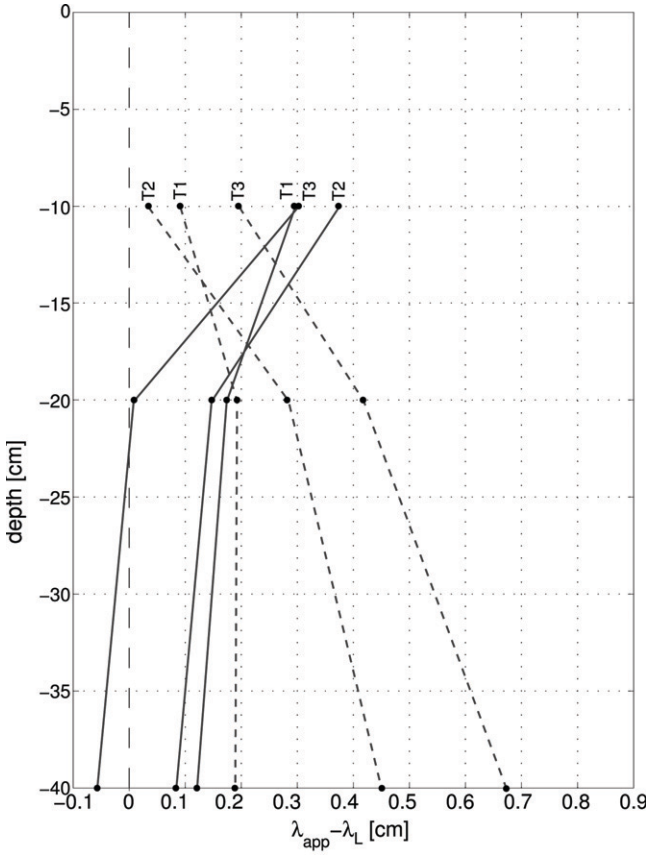


Fig. 13. Difference of apparent dispersivity length $\lambda_{app}$ to soil dispersivity length $\lambda_L$ at three soil depth ($z$ = −10, −20, −40 cm) for three transpiration rates T1 = 0.25 cm d$^{-1}$, T2 = 0.5 cm d$^{-1}$, and T3 = 0.667 cm d$^{-1}$, with solute exclusion (dashed) and passive solute uptake (continuous).

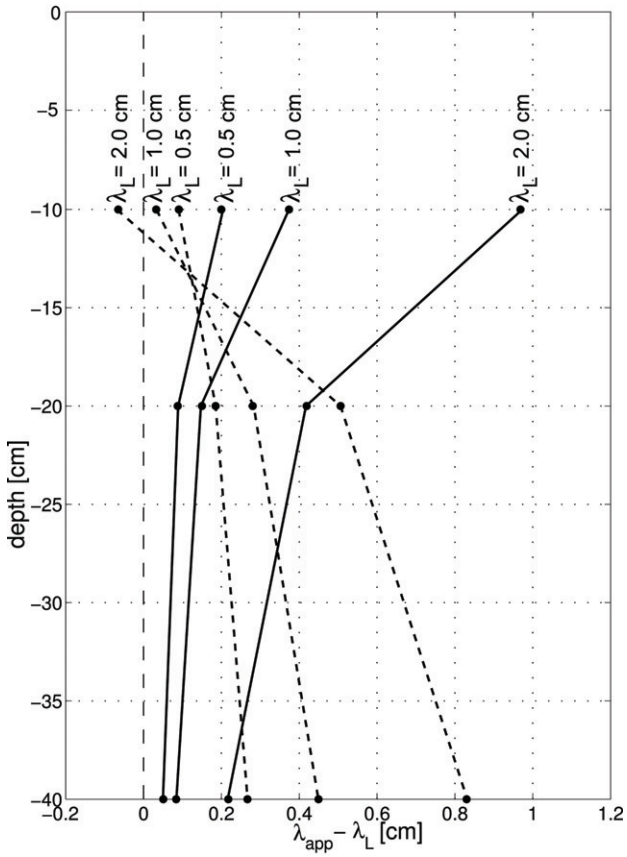


Fig. 14. Difference of apparent dispersivity length $\lambda_{app}$ minus different soil dispersivity length $\lambda_L$ at three soil depths ($z$ = −10, −20, −40 cm) for the fibrous root system with transpiration rate $T_{pot}$ = 0.5 cm d$^{-1}$; passive solute uptake (continuous) and solute exclusion (dashed).

the difference between the apparent and soil dispersivity length versus soil depth. If solute is excluded, the largest relative effect on the apparent dispersivity length can be seen for the lowest soil dispersivity length ($\lambda_L$ = 0.5 cm), while for passive solute uptake the largest relative effect is seen for the largest $\lambda_L$ (2 cm). The difference decreased with depth when solute was taken up passively and vanished at soil depth without plant roots (z = −40 cm), where almost no impact of soil dispersivity length was seen. The results show that for both solute uptake definitions (solute exclusion and passive uptake), the difference between apparent dispersivity and soil dispersivity increased with increasing soil dispersivity. This is different from the effect that soil dispersivity has on the apparent dispersivity in soils with spatially variable soil hydraulic properties. Using approximate solutions of stochastic transport equations, Fiori (1996) demonstrated that soil dispersivity, which is also called local dispersivity, has no impact on the difference between the apparent and soil dispersivities for small soil dispersivities. For larger local dispersivity, this difference even decreases with increasing local dispersivity. This shows that the effects of root water and nutrient uptake on $\lambda_{app}$ are different and not additive compared to the effect of soil heterogeneity.

## Scenario 4: Impact of Transient Flow

The upper boundary condition of the plant collar was changed from a constant to a transient flow (Fig. 3). The solute setup did not change, and no solute uptake (exclusion) was defined. The breakthrough curves of both, transient and constant boundary conditions, are compared in Fig. 15. As there is no uptake during the night, the net vertical water flux is downward, while in the middle of the day, as the instantaneous transpiration is higher than the rainfall, the flux goes to the root system. This generates the diurnal oscillation of the solute concentration in the upper root zone, while in the lower soil the effect of transient flow fades out. Below the root zone ($z$ = −40 cm) no difference between BTCs, either simulated with a constant or a transient collar flux, could be seen anymore.

The effect of the transient flow regime on the apparent dispersivity length depended strongly on the root structure and depth (Fig. 16). For both root systems, the effect of transient flow conditions decreased with increasing depth. For the fibrous system, transient flow led to larger apparent dispersivity values when compared with steady-state flow close to the soil surface, whereas the opposite was observed for the taprooted system. Below of the root zone ($z$ =

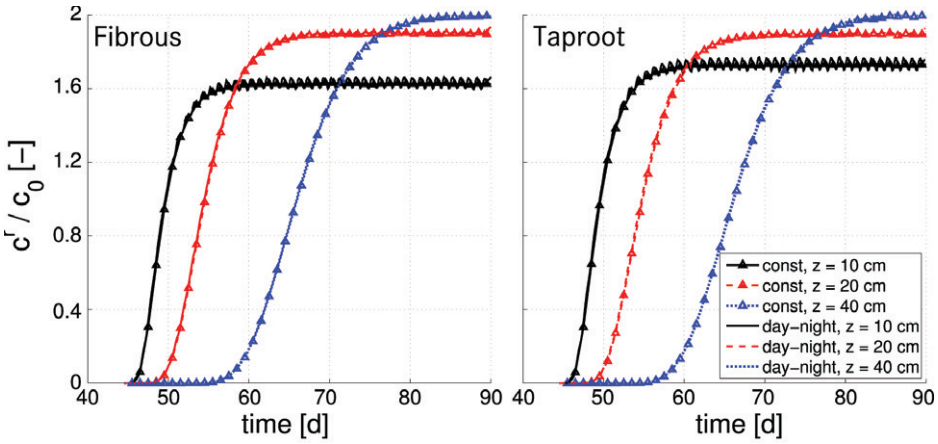


Fig. 15. Three-dimensionally simulated breakthrough curves at $z = -10$, $-20$, and $-40$ cm of the soil column with root water uptake by a (left) fibrous and a (right) taprooted root structure; root transpiration compared between constant collar flux and diurnal root water uptake with $T_{pot} = 0.5$ cm d$^{-1}$; solute boundary condition at the top: $c_0 = 10^{-2}$ μmol cm$^{-3}$; the scenario was run with solute exclusion.

−40 cm), the apparent dispersivity values of both plants and both boundary conditions of the plant collar were in the same range.

## Summary and Conclusions

Several simulation experiments were run to investigate the impact of root water and solute uptake on solute transport in soil. In these scenarios parameters and steady boundary conditions were varied, and the apparent dispersivity length, which is used as a characteristic of solute spreading in soil, was estimated by fitting solute breakthrough curves with the one-dimensional model HYDRUS-1D. The results showed deviations of the apparent dispersivity lengths from the soil dispersivity values used in the three-dimensional simulations.

The taprooted and fibrous root architectures, with similar root length density profiles and a similar total root length, resulted in similar profiles of the mean average vertical pore water velocity but different profiles of the coefficient of variation of the pore water velocity, and water sink term distributions (Fig. 5). When compared with apparent dispersivity length derived from simulations with a constant transpiration rate, the diurnal cycles of the transpiration rate influenced the apparent dispersivity length only in the soil layers with diurnal cycles of water content. This effect might be due to the upward total flux during the day and decreased with increasing soil depths. Below the root zone, the difference vanished.

Besides the root water uptake, the solute uptake mechanism has an important impact on solute transport. Different solute uptake mechanisms led to different redistributions of the solute mass in the heterogeneous flow field that was generated by the root water uptake. This solute redistribution also had an important impact on the apparent dispersivity length and its behavior with travel distance, and this impact depended on the root architecture.

In our simulations we considered a homogeneous soil and found that it led to higher apparent dispersivity values for passive uptake and solute exclusion. This contrasts previous simulations in heterogeneous soils where the apparent dispersivity decreased due to plant water uptake Russo et al. (1998). In our study, the effect of

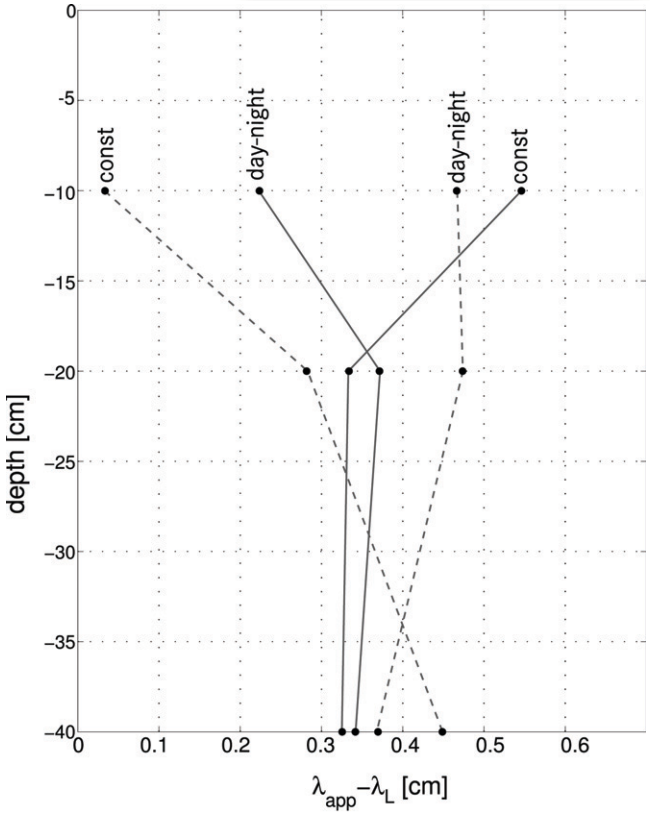


Fig. 16. Difference of apparent dispersivity length $\lambda_{app}$ minus soil dispersivity length $\lambda_L$ at three soil depth ($z = -10$, $-20$, $-40$ cm) for a constant and a transient collar flux; fibrous (dashed) and taproot (continuous).

water uptake by individual roots on the flow field was considered, whereas in Russo et al. (1998), spatial variability of root water uptake was described on a macroscopic scale, so that its effect on the smaller scale was not explicitly simulated.

For active solute uptake, we also noticed that solute uptake rate parameters that have been determined in nutrient solutions cannot be transferred to simulate nutrient uptake in soils using bulk soil concentrations. It should be noted that we only considered nonsorbing solutes. For sorbing solutes, concentration gradients close to the root surface are larger than for nonsorbing solutes, so this

effect will be even larger for these substances. These dependencies illustrate that the dispersivity length that is used in one-dimensional simulation models should not be considered as a soil property since it depends on flow conditions and root and plant properties. To what extent these dependencies need to be considered in practical applications such as simulations for prediction of leaching plant nutrients and plant protection products out of the root zone requires further investigation.

In this study we focused on transport in a homogeneous soil in which root water and solute uptake were the only processes that generated solute redistribution and flow field heterogeneity and therefore influenced the apparent dispersivity. Soil heterogeneity also plays an important role, and its impact on flow field heterogeneity and the magnitude and scale dependency of the apparent dispersivity have been investigated intensively (e.g., Vanderborght et al., 2006). A review of apparent dispersivities that were derived from leaching experiments in undisturbed bare soils indicated that, in general, the apparent dispersivity increases from 2 cm for a travel distance of 20 to 6 cm for a travel distance of 100 cm (see Fig. 6 in Vanderborght and Vereecken, 2007). Assuming a simple linear relation between travel distance and apparent dispersivity, dispersivity would increase from 2 to 3 cm (i.e., by 50%) for an increase of travel distance from 20 to 40 cm. Although we do not want to put much weight on this very simple analysis, it nevertheless illustrates that the effect of root water and nutrient uptake on the apparent dispersivity, which may also lead to an increase of apparent dispersivity by 50% over the same transport distance depending on the considered scenario, does not seem negligible when compared with the effect of soil heterogeneity. The effects of root water and nutrient uptake and soil heterogeneity on apparent dispersivity are not expected to be additive since interactions between root water uptake and the spatially variable water contents and water fluxes in a heterogeneous soil are plausible.

In future studies, the virtual experiments could be extended to simulations in heterogeneous soil. In addition, simulations with different horizontal root length density (increasing and decreasing of soil domain but with the same root structure) and simulations with similar plants, but different potential transpiration rates (heterogeneous water uptake) could identify important effects on solute movements in soil.

In our simulations, we considered cases with a high leaching rate, when compared with expected leaching rates in field soils, and with a quasi-steady flow regime. Such conditions may be relevant for experimental conditions of leaching experiments or for regularly (over)irrigated crops. Another scope of additional simulation experiments could be to investigate the interactions between plant water and solute uptake and transport under more natural climatic boundary conditions leading to lower ratios of the leaching rate to the rainfall/irrigation rate at the soil surface and to a larger time scale (i.e., seasonal time scale) of the temporal variation of leaching rates. For those conditions water uptake profiles may vary considerably over time when parts of the root zone dry out and root water uptake is locally reduced. Differences in modeled profiles of root water uptake by three-dimensional and one-dimensional models in these cases also are expected to have an impact on simulated solute transport.

Since theses studies are limited to simulation experiments, the results should also be validated with experimental data. Therefore, tracer measurements in soil with plants and root water uptake, using magnetic resonance imaging, will be performed. Comparing these experiments with our simulated data could lead to a better understanding of the effects on solute movement by root water and solute uptake.

## References


Bear, J. 1972. Dynamics of fluids in porous media. American Elsevier, New York.

Bechtold, M., J. Vanderborght, O. Ippisch, and H. Vereecken. 2011. Efficient random walk particle tracking algorithm for advective-dispersive transport in media with discontinuous dispersion coefficients and water content. Water Resour. Res. 47:W10526. doi:10.1029/2010WR010267

Doussan, C., A. Pierret, E. Garrigues, and L. Pagès. 2006. Water uptake by plant roots: II—Modelling of water transfer in the soil root-system with explicit account of flow within the root system—Comparison with experiments. Plant Soil 283:99–117. doi:10.1007/s11104-004-7904-z

Draye, X., Y. Kim, G. Lobet, and M. Javaux. 2010. Model-assisted integration of physiological and environmental constraints affecting the dynamic and spatial patterns of root water uptake from soils. J. Exp. Bot. 61:2145–2155. doi:10.1093/jxb/erq077

Fiori, A. 1996. Finite Peclet extensions of Dagan's solutions to transport in anisotropic heterogeneous formations. Water Resour. Res. 32:193–198. doi:10.1029/95WR02768

Gish, T.J., and W.A. Jury. 1983. Effect of plant roots and roots channels on solute transport. Trans. ASABE 26(2):440–444.

Green, S., M. Kirkham, and B. Clothier. 2006. Root uptake and transpiration: From measurements and models to sustainable irrigation. Agric. Water Manage. 86:165–176. doi:10.1016/j.agwat.2006.06.008

Hammel, K., J. Gross, G. Wessolek, and K. Roth. 1999. Two-dimensional simulation of bromide transport in a heterogeneous field soil with transient unsaturated flow. Eur. J. Soil Sci. 50:633–647. doi:10.1046/j.1365-2389.1999.00273.x

Hopmans, J.W., and K.L. Bristow. 2002. Current capabilities and future needs of root water and nutrient uptake modeling. Adv. Agron. 77:103–183. doi:10.1016/S0065-2113(02)77014-4

Javaux, M., J. Vanderborght, R. Kasteel, and M. Vanclooster. 2006. Three-dimensional modeling of the scale- and flow rate dependency of dispersion in a heterogeneous unsaturated sandy monolith. Vadose Zone J. 5:515–528. doi:10.2136/vzj2005.0056

Javaux, M., T. Schröder, J. Vanderborght, and H. Vereecken. 2008. Use of a three-dimensional detailed modeling approach for predicting root water uptake. Vadose Zone J. 7:1079–1089. doi:10.2136/vzj2007.0115

Pagès, L., G. Vercambre, J. Drouet, F. Lecompte, C. Collet, and J. Le Bot. 2004. Root Typ: A generic model to depict and analyse the root system architecture. Plant Soil 258:103–119. doi:10.1023/B:PLSO.0000016540.47134.03

Richards, L.A. 1931. Capillary conduction of liquids through a porous medium. Physics 1:318–333. doi:10.1063/1.1745010

Roose, T., and G.J.D. Kirk. 2009. The solution of convection–diffusion equations for solute transport to plant roots. Plant Soil 316:257–264. doi:10.1007/s11104-008-9777-z

Russo, D., J. Zaidel, A. Fiori, and A. Laufer. 2006. Numerical analysis of flow and transport from a multiple-source system in a partially saturated heterogeneous soil under cropped conditions. Water Resour. Res. 42:W06415. doi:10.1029/2006WR004923

Russo, D., J. Zaidel, and A. Laufer. 1998. Numerical analysis of flow and transport in a three-dimensional partially saturated heterogeneous soil. Water Resour. Res. 34:1451–1468. doi:10.1029/98WR00435

Russo, D., J. Zaidel, and A. Laufer. 2004. Numerical analysis of flow of interacting solutes in a three-dimensional unsaturated heterogeneous soil. Vadose Zone J. 3:1286–1299.

Schröder, T., M. Javaux, J. Vanderborght, B. Krfgen, and H. Vereecken. 2008. Effect of local soil hydraulic conductivity drop using a three-dimensional root water uptake model. Vadose Zone J. 7:1089–1098. doi:10.2136/vzj2007.0114

Schröder, T., M. Javaux, J. Vanderborght, B. Krfgen, and H. Vereecken. 2009. Implementation of a microscopic soil–root hydraulic conductivity drop function in a three-dimensional soil–root architecture water transfer model. Vadose Zone J. 8:783–792. doi:10.2136/vzj2008.0116

Šimůnek, J., and J. Hopmans. 2009. Modeling compensated root water and nutrient uptake. Ecol. Modell. 220:505–521. doi:10.1016/j.ecolmodel.2008.11.004

Simůnek, J., K. Huang, and M.Th. van Genuchten. 1995. The SWMS_3D code for simulating water flow and solute transport in three-dimensional variably saturated media. V. 1.0. Research Rep. 139. USDA-ARS, U.S. Salinity Lab, Riverside, CA.

Simůnek, J., M. Šejna, H. Saito, M. Sakai, and M.Th. van Genuchten. 2008. The HYDRUS-1D software package for simulating the movement of water, heat, and multiple solutes in variably saturated media. Version 4.0, HYDRUS Software Series 3. Dep. Environmental Sci., Univ. of California, Riverside.

Tompson, A.F.B., and L.W. Gelhar. 1990. Numerical simulation of solute transport in three-dimensional, randomly heterogeneous porous media. Water Resour. Res. 26:2541–2562. doi:10.1029/WR026i010p02541

Vanderborght, J., R. Kasteel, M. Herbst, M. Javaux, D. Thiéry, M. Vanclooster, C. Mouvet, and H. Vereecken. 2005. A set of analytical benchmarks to test numerical models of flow and transport in soil. Vadose Zone J. 4:206–221.

Vanderborght, J., R. Kasteel, and H. Vereecken. 2006. Stochastic continuum transport equations for field-scale solute transport: Overview of theoretical and experimental results. Vadose Zone J. 5:184–203. doi:10.2136/vzj2005.0024

Vanderborght, J., D. Mallants, and J. Feyen. 1998. Solute transport in a heterogeneous soil for boundary and initial conditions: Evaluation of first-order approximations. Water Resour. Res. 34:3255–3270. doi:10.1029/98WR02685

Vanderborght, J., and H. Vereecken. 2007. Review of dispersivity lengths for transport modeling in soils. Vadose Zone J. 6:27–51.

van Genuchten, M.Th. 1980. A closed-form equation for predicting the hydraulic conductivity of unsaturated soils. Soil Sci. Soc. Am. J. 44:892–898.

Vereecken, H., T. Kamai, T. Harter, R. Kasteel, J. Hopmans, and J. Vanderborght. 2007. Explaining soil moisture variability as a function of mean soil moisture: A stochastic unsaturated flow perspective. Geophys. Res. Lett. 34:0–5.

Vogeler, I., S.R. Green, D.R. Scotter, and B.E. Clothier. 2001. Measuring and modelling the transport and root uptake of chemicals in the unsaturated zone. Plant Soil 231:161–174. doi:10.1023/A:1010337132309

Yang, J.Z., R.D. Zang, J.Q. Wu, and M.B. Allen. 1996. Stochastic analysis of adsorbing solute transport in two-dimensional unsaturated soils. Water Resour. Res. 32:2747–2756. doi:10.1029/96WR01101